Supplementary Information

for

Synthesis, crystal structure from PXRD of a $Mn^{II}(purp)_2$ complex, interaction with DNA at different temperature, pH and lack of stimulated ROS formation by the complex

Bitapi Mandal, Soumen Singha, Sanjay Kumar Dey, Swagata Mazumdar, Parimal Karmakar, Tapan Kumar Mondal, Sanjay Kumar, Saurabh Das*

Experimental:

Determination of stoichiometry of the Mn^{II} complex of purpurin (LH_3)

Mole-ratio method:

Concentration of Mn^{II} was constant while LH_3 was varied and vice-versa. The change in absorbance was measured at 513 nm and plotted against ratio of LH_3 to Mn^{II} [Fig. S1(a)] and ratio of Mn^{II} to LH_3 [Fig. S1(b)]. Straight lines were obtained whose intersection helped to determine stoichiometry of the complex formed in solution.

Job's method of continuous variation:

Stoichiometry was also determined by continuously varying the concentrations of both ligand and the metal ion [Fig. S1(c)].

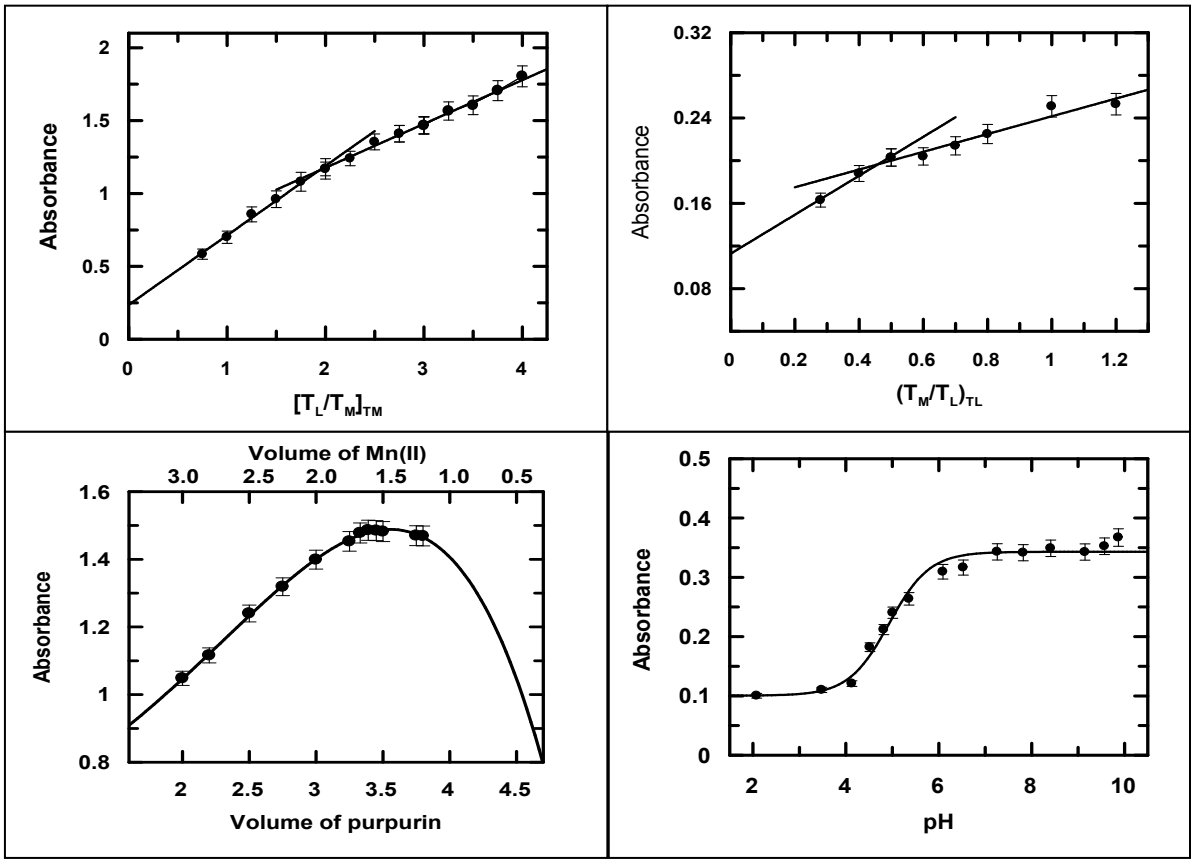

Fig. S1: (a) and (b): Mole-ratio plot showing the interaction of Mn^{II} with purpurin in solution at neutral pH; (c): Job's plot of continuous variation showing the interaction of Mn^{II} with purpurin at neutral pH. (d) Spectrophotometric titration of purpurin in the presence of Mn^{II} in the ratio 2:1 as shown by the variation of absorbance at 513 nm; $[NaNO_3]$ = 100 mM, T = 298 K.

Both methods suggest the formation of a 1:2 metal-ligand complex at neutral pH.

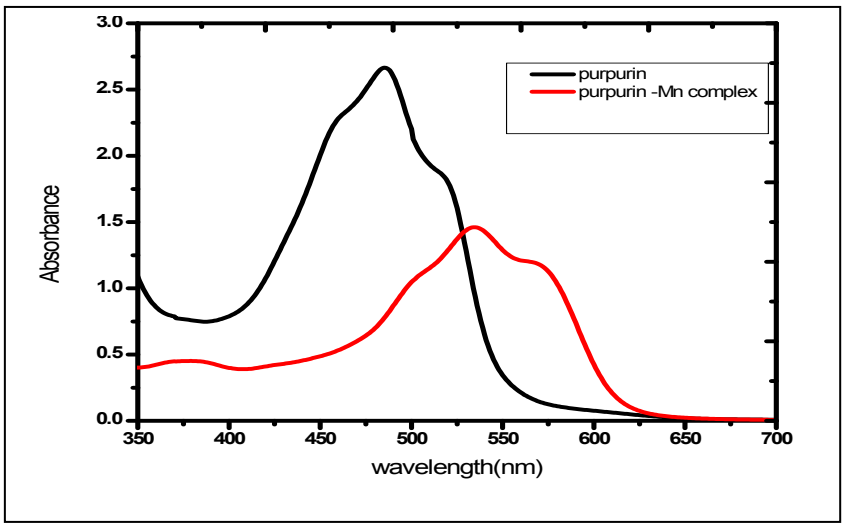

Fig. S2: UV-Vis spectra of purpurin and its Mn^{II} complex in DMSO

Analysis of IR spectra:

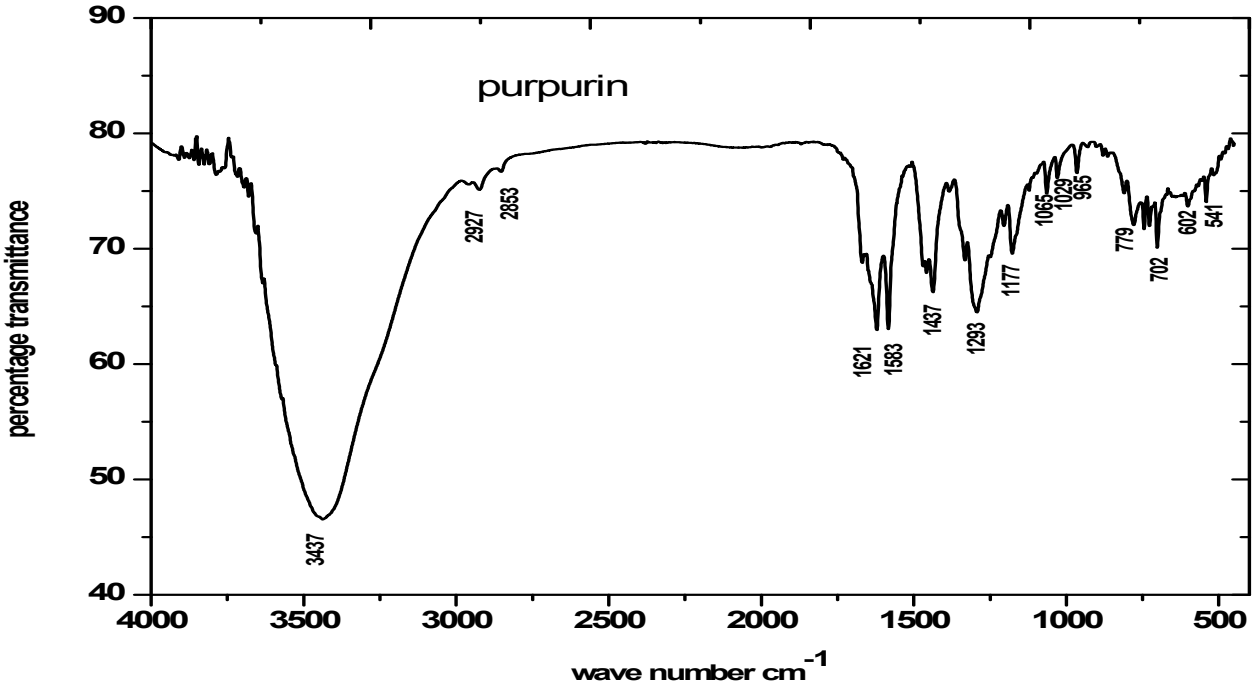

Fig. S3: IR spectra of purpurin

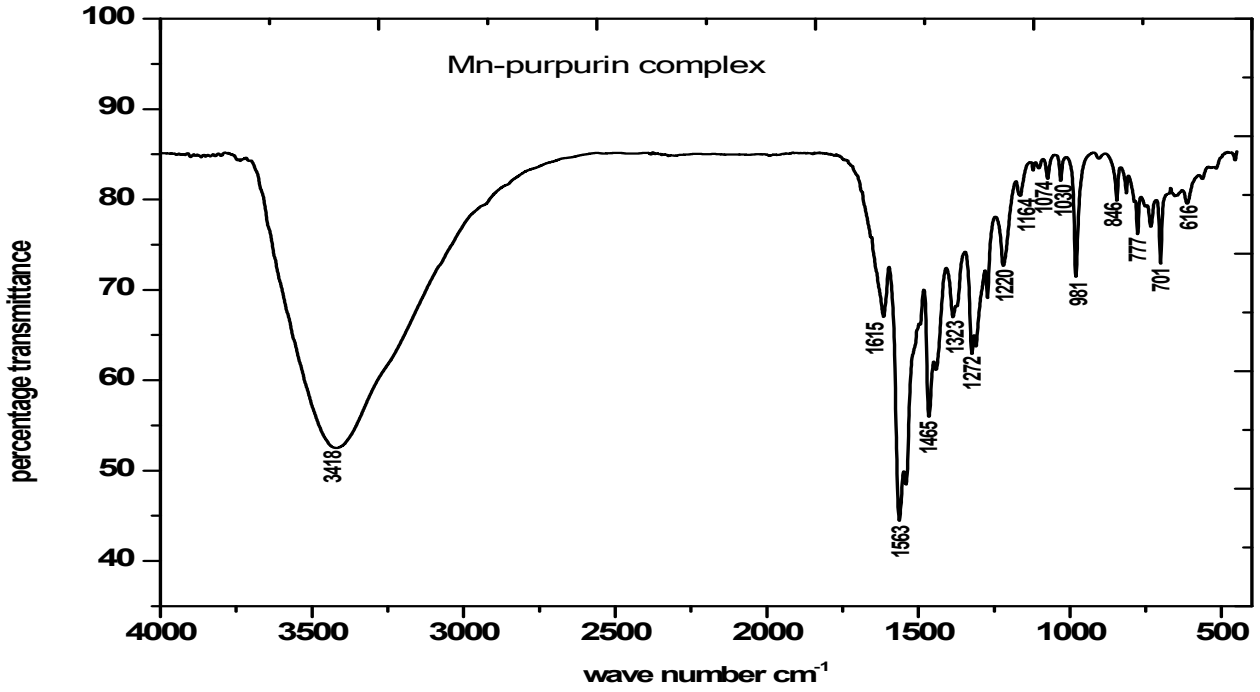

Fig. S4: IR spectrum of $Mn^{(II)}(LH_2)_2$.

Fig. S3 is IR spectrum of purpurin showing a broad peak at 3437 cm^{-1} characteristic of O–H stretching which was also found in the complex at ~3418 cm^{+-1} (Fig. S4). This is because like in purpurin the complex also possesses free OH groups (two on each ligand) other than the one that binds the metal ion. Hence, response for OH stretching remains almost unaltered. IR spectra of purpurin shows a characteristic peak for carbonyl at 1621 cm^{-1} that disappeared completely in the complex suggesting the participation of carbonyl oxygen in binding the metal ion. Peaks at 1621 cm^{-1} and 1583 cm^{-1} in the IR spectra of purpurin is attributed to C=O str. due to carbonyl and C=C str. due to double bonds respectively or a combination of both. This region showed distinct changes in the IR spectra of the complex with a new peak at 1563 cm^{-1}. Peaks obtained in the region 1437 cm^{-1} to 965 cm^{-1} for purpurin is attributed to a combination of OH and CH

bending modes. Nature of peaks in this region is different in the complex. New peaks were found at 981 cm^{-1} and 701 cm^{-1} indicating the formation of an Mn─O bond.

Mass Spectrum:

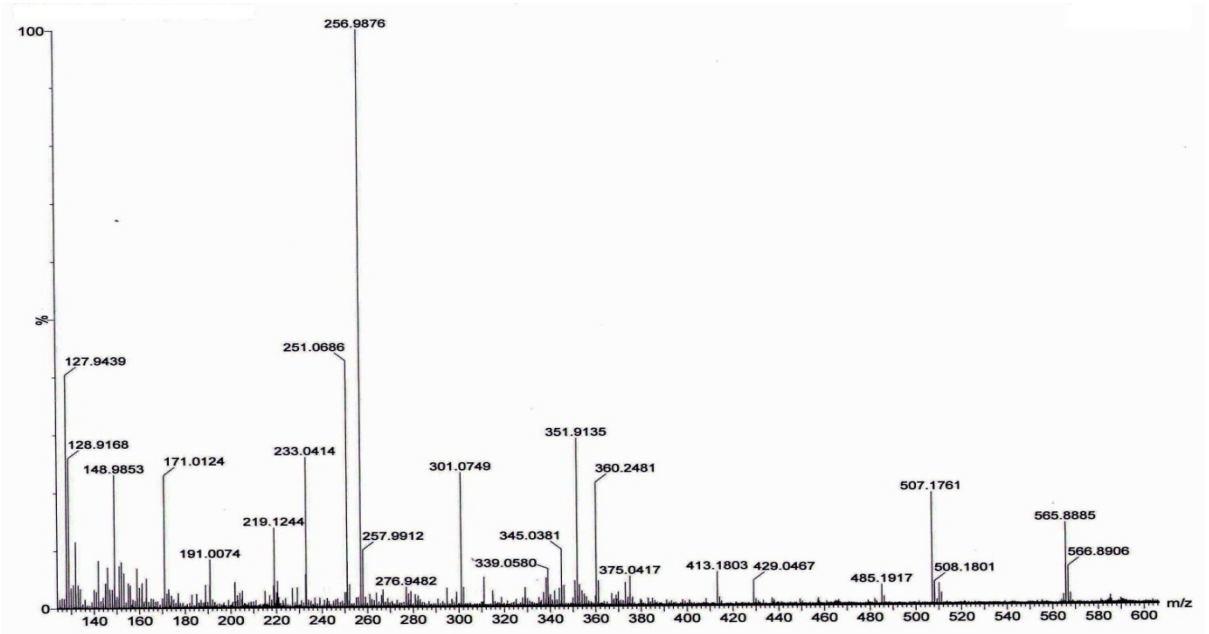

Fig. S5: Mass spectrum of $Mn^{(II)}(LH_2)_2$

Analysis of Mass spectrum:

The molecular ion peak was detected at m/z = 565.88 and 566.89 (m/z_{theo} = 565.32). The peak found at m/z = 485.19 corresponds to the fragment formed from the molecular ion by loss of a butadiene unit (from anyone of the ligands), an OH group and an unbound carbonyl oxygen. The peak at m/z = 413.18 corresponds to the fragment formed by loss of two butadiene units (one from each ligand), three hydroxyl groups and four aromatic hydrogens from the molecular ion. Elimination of two carbonyl oxygen along with a hydroxyl group from the molecular ion provides a peak at m/z = 507.17 or 508.18. The peak at m/z = 256.98, is that of a purpurin that

breaks away from the complex. The other portion i.e. Mn^{II} bound to only one purpurin was also found at m/z = 311.3.

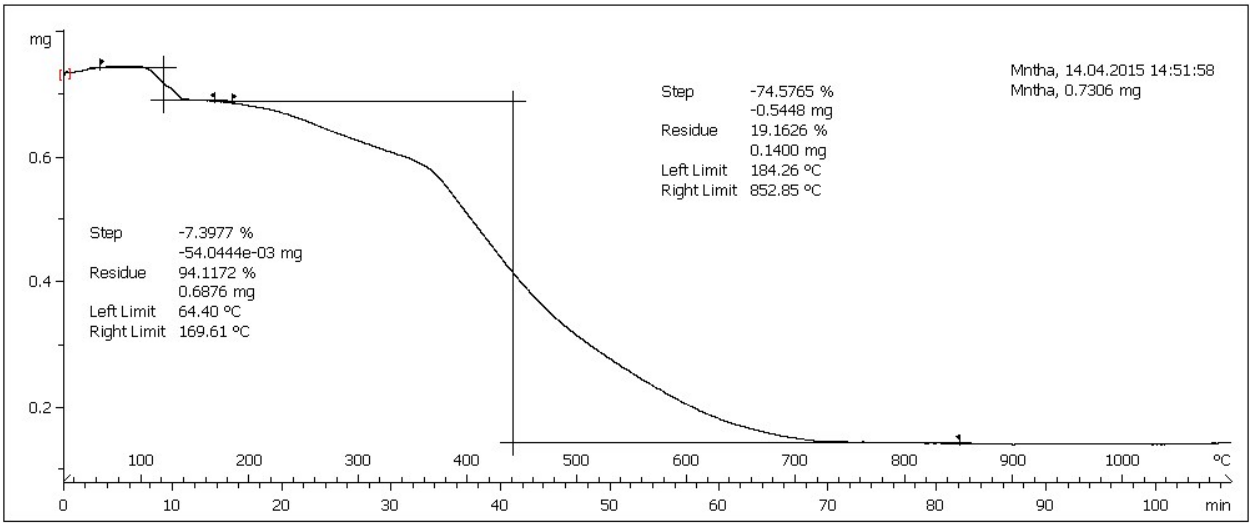

Fig. S6: A routine thermo-gravimetric analysis plot for the Mn^{II}-purpurin complex

Thermo-gravimetric analysis:

Experimental loss in weight at 120°C is 5.89 %. Considering two molecules of water to be associated with the complex the percentage loss of water is 5.98 %. Hence TGA suggests the presence of two molecules of water in the complex which was also found for the structure obtained from PXRD data.

Interaction of the compounds with DNA

Binding of the compounds with c t DNA was studied considering the following equilibrium

$$L + DNA \rightleftharpoons L - DNA \qquad K_d = \frac{[L][DNA]}{[L - DNA]} \qquad \text{(S1)}$$

Equation S1 considered in the reverse direction yields a double reciprocal Equation S2.

$$\frac{1}{\Delta A} = \frac{1}{\Delta A_{max}} + \frac{K_d}{\Delta A_{max}(C_D - C_L)} \quad \text{(S2)}$$

Decrease in absorbance (ΔA) upon titrating the complex with c t DNA was used to create binding isotherms at different pH [1-4]. ΔA_{max} indicates the maximum change in absorbance following interaction of the complex with c t DNA. C_D denotes the concentration of c t DNA and C_L the concentration of the complex. K_d and ΔA_{max} was evaluated utilizing Eq. S2.

Change in absorbance was followed at the λ_{max} of the complex at all pH in which experiments were done. In the pH range 7.19 to 8.25, change in absorbance (ΔA) was followed at 513 nm. Fig. S7 is a typical double reciprocal plot from where K_d and ΔA_{max} are evaluated using Eq. S2. A plot of $\Delta A/\Delta A_{max}$ against the concentration of DNA was fitted using non-linear curve fit analysis (Eq. S3 & S4) and K_d was evaluated at all experimental pH.

$$K_d = \frac{\left[C_L - \left(\frac{\Delta A}{\Delta A_{max}}\right)C_L\right]\left[C_D - \left(\frac{\Delta A}{\Delta A_{max}}\right)C_L\right]}{\left(\frac{\Delta A}{\Delta A_{max}}\right)C_L} \quad \text{(S3)}$$

$$C_L\left(\frac{\Delta A}{\Delta A_{max}}\right)^2 - (C_L + C_D + K_d)\left(\frac{\Delta A}{\Delta A_{max}}\right) + C_D = 0 \quad \text{(S4)}$$

The plot of $\Delta A/\Delta A_{max}$ against [DNA]/[$Mn^{II}(LH_2)$] at different pH was done to obtain " n_b " the site size of interaction [Fig. S8]. The overall binding constant (K*) at each pH was obtained by multiplying K_{app} (obtained using Eq. S2 and Eqs. S3 & S4) with "n_b".

A modified form of the original Scatchard equation (Eq. S5) [5] was also used to analyze the results. Overall binding constant (K*) and binding stoichiometry "n" (= n_b^{-1}) were obtained directly [1, 6] from Fig. 6.

$$r/C_f = K^*(n - r) \quad \text{(S5)}$$

r = C_b/C_D where, "C_b" is the concentration of bound complex and "C_D" the concentration of c t DNA. "C_f" refers to concentration of free complex in solution. K* is the intrinsic or overall binding constant of the complex binding to a substrate. "n" is the binding stoichiometry in terms of the number of bound complex per nucleotide while "n_b" reciprocal of "n" denotes the binding site size in terms of the number of nucleotide bound to the complex.

Cell culture and cell viability assay

MOLT-4 cells were cultured in RPMI medium (GIBCO, Invitrogen, Carlsbad, CA, US), supplemented with 10% fetal bovine serum (GIBCO), antibiotic mixture (1X) PSN (GIBCO) and gentamicin reagent solution (GIBCO). Cells were incubated in a humidified CO_2 incubator at 37^{o}C and seeded in 96 well plates for 24 hours prior to drug treatment. After 24 hours, cells were treated with purpurin, $Mn^{II}(Purp)_2$ that were earlier dissolved in DMSO. Concentration of DMSO was less than 0.5%. After treatment for 72 hours, cell viability was checked by 3-(4,5-dimethylthiazol-2-yl)-2,5-diphenyltetrazolium bromide (MTT) assay. Briefly, cells were washed with 1X PBS and treated with MTT for 4 hours at 37^{o}C. Precipitates were dissolved in DMSO and plates were analyzed on a Thermo MULTISKAN EX plate reader at 595 nm.

Results and Discussion:

The initial structural model for $Mn^{II}(LH_2)_2$ that was used to arrive at the structure of the complex from PXRD data is provided below:

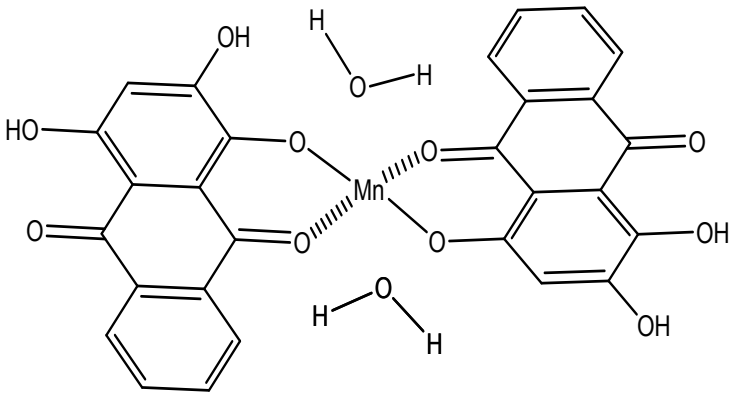

DFT computations were done to establish the structure of the complex. Ground state electronic structure calculations were carried out using the DFT method [9]. Based on the optimized ground state geometry, the absorption spectral properties in ethanol were calculated by time-dependent density functional theory (TDDFT) method. All calculations were performed with Gaussian 09W software package [10]. GaussSum 2.1 program was used to calculate the molecular orbital contributions from groups or atoms.

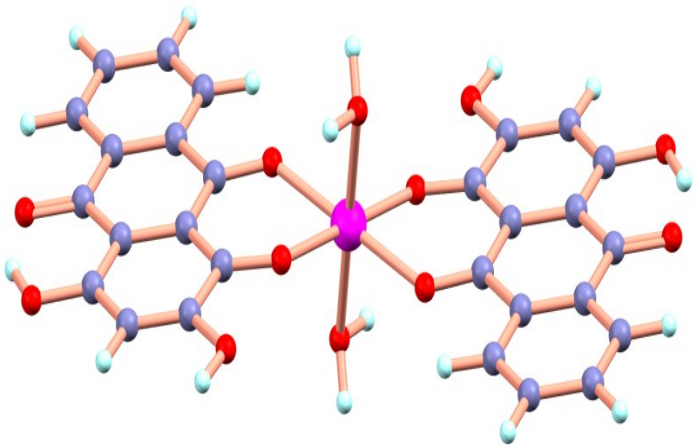

Optimized structure in octahedral, high spin state (S = 5/2)

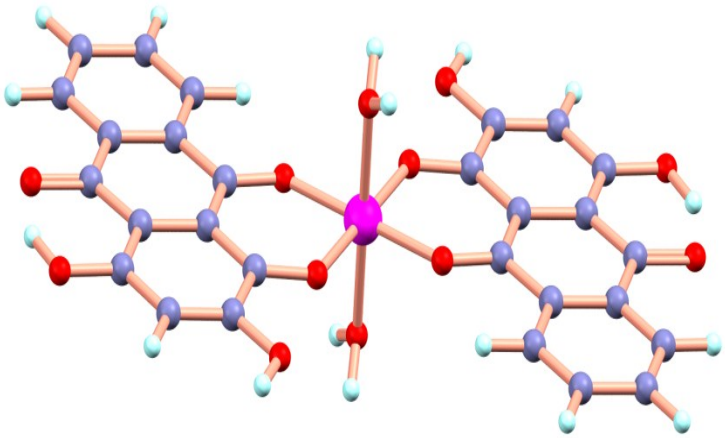

Optimized structure in octahedral, low spin state (S = 1/2)

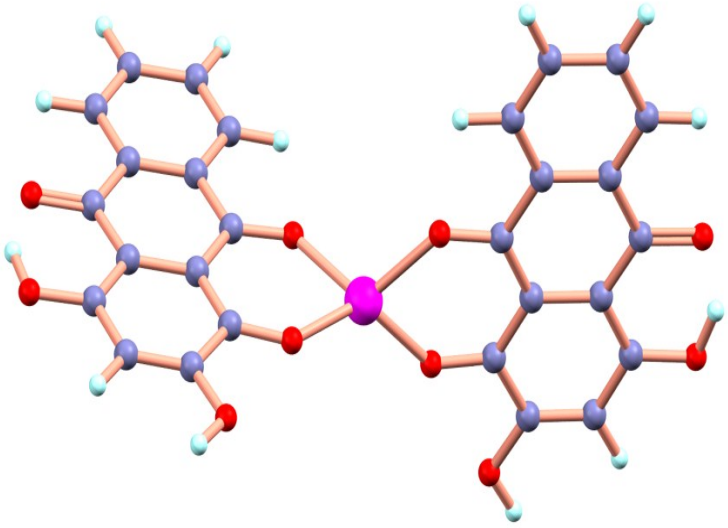

Optimized structure in tetrahedral, high spin state (S = 5/2)

Relative Energy:

Octahedral high spin state = 0.0 kcal/mol (Most stable structure)

Octahedral low spin state = 29.178 kcal/mol

Tetrahedral high spin state = 29.163 kcal/mol

Determination of stability constant of $Mn^{(II)}(LH_2)_2$ in solution:

The stability constant for the formation of the complex was determined with the help of a spectrophotometric titration where Mn^{II} and purpurin were taken in the ratio 1:2. Change in absorbance at 513 nm in the pH range 2.08 to 6.53 revealed there was a gradual increase in pH initially up to 4.13; beyond this there was an abrupt increase at pH 4.52. Beyond 4.52, the increase in absorbance was again gradual but much more prominent than in the range mentioned earlier. In the pH range, 4.5 to 6.2, a proton from the –OH group at C_1 got ionized (Eq. 1) [7].

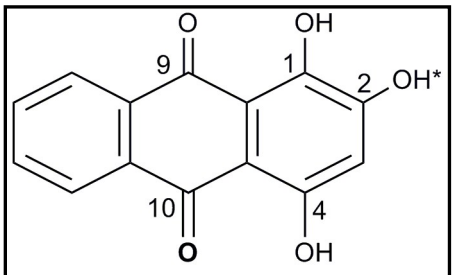

Purpurin or LH_3 or LH_2H^*

$$LH_2H^* \rightleftharpoons LH^*H^- + H^+ \qquad \text{(S6)}$$

The deprotonated LH_2H^* reacts with Mn^{II} according to equilibrium shown by Eq. S7.

$$Mn^{2+} + 2\ LH_2H^* \rightleftharpoons Mn(LH^*H)_2 + 2H^+ \qquad \text{(S7)}$$

The change in absorbance (A_{obs}) at 513 nm was fitted according to Eq. 3 (main text):

A_1 and A_2 in Eq. 3 refer to the absorbance of LH_2H^* and LH^*H^- respectively in the presence of Mn^{II}. Fitting the experimental data according to Eq. 3 [Fig. S1 (d)], pK_a was found to be 4.897 ± 0.11. Using this value and Eqs. S8-S11, the stability constant of the complex in solution was determined [1, 6, 8].

$$\beta^* = \frac{[Mn(LH_2)_2][H^+]^2}{[Mn^{2+}][LH_3]^2} \qquad \text{(S8)}$$

$$Mn^{2+} + 2LH_2^- \rightleftharpoons Mn(LH_2)_2 \quad \text{(S9)}$$

$$\beta = \frac{[Mn(LH_2)_2]}{[Mn^{2+}][LH_2^-]^2} \quad \text{(S10)}$$

$$\beta = \frac{\beta^*}{K^2} \quad \text{(S11)}$$

K refers to the equilibrium constant for the dissociation of the phenolic-OH of LH_3 at C_1 when titrated alone [1]. The value for the formation constant (β) determined using Eq. S11 was found to be 1.1×10^{18} and is comparable to the reported stability constants of Cu^{II} with doxorubicin [$(4.6 \pm 1.1) \times 10^{16}$] and with sodium 1,4-dihydroxy-9,10-anthraquinone-2-sulphonate [9.64×10^{16}] [2,4].

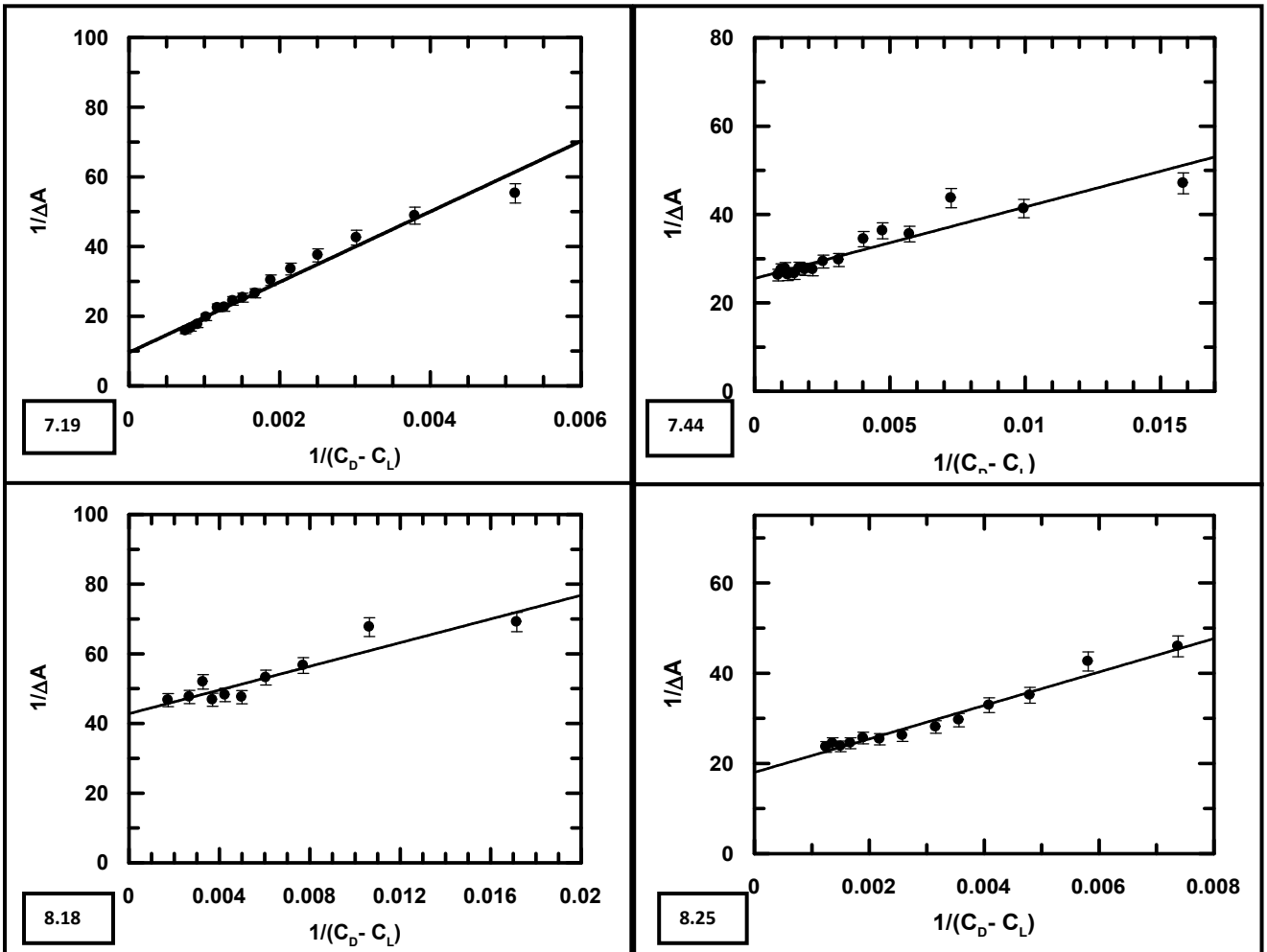

Figure S7: Double reciprocal plots for $Mn^{II}(purp)_2$ complex titrated with calf thymus DNA at different pH.

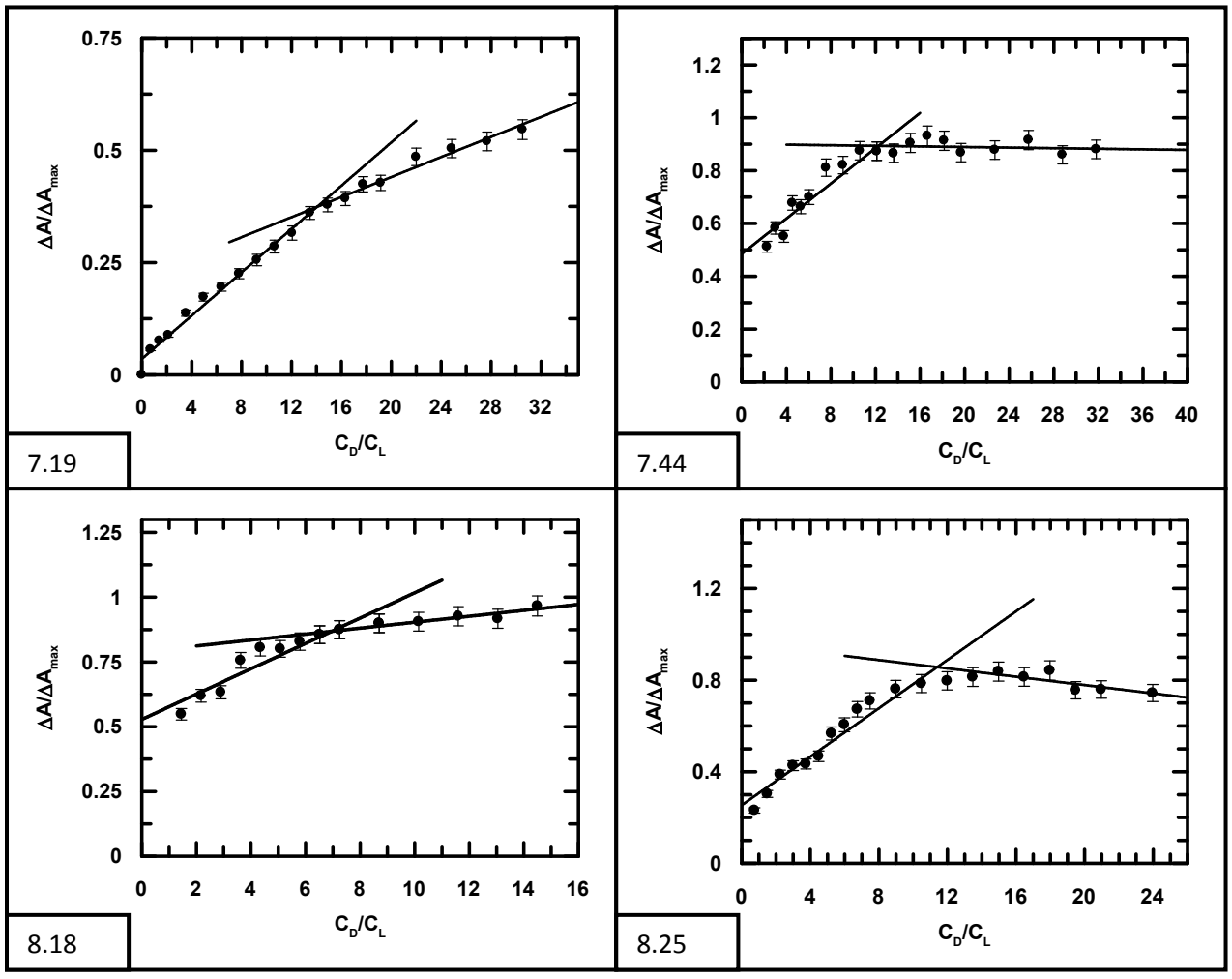

Fig. S8: Plots for the normalized increase in absorbance as a function of mole-ratio of c t DNA to the complex at four different pH.

Cell viability assay

The study revealed that the complex was slightly better in killing MOLT-4 cells having an IC_{50} value of 26.5 μM. The same for purpurin is 29.0 μM. The data suggests $Mn^{II}(LH_2)_2$ was marginally more potent than purpurin (Fig. S9). Such a finding in favor of the complex is interesting because it is observed in spite of decreased ROS generation by it suggesting that the complex is able to maintain the performance of purpurin on MOLT-4 cells, rather improve things slightly. Hence, the presence of the metal ion in the complex probably equips it to impair other cellular processes making up for the disadvantage that it faces with regard to efficacy due to decreased ROS formation due to it, in affecting cellular damage compared to purpurin.

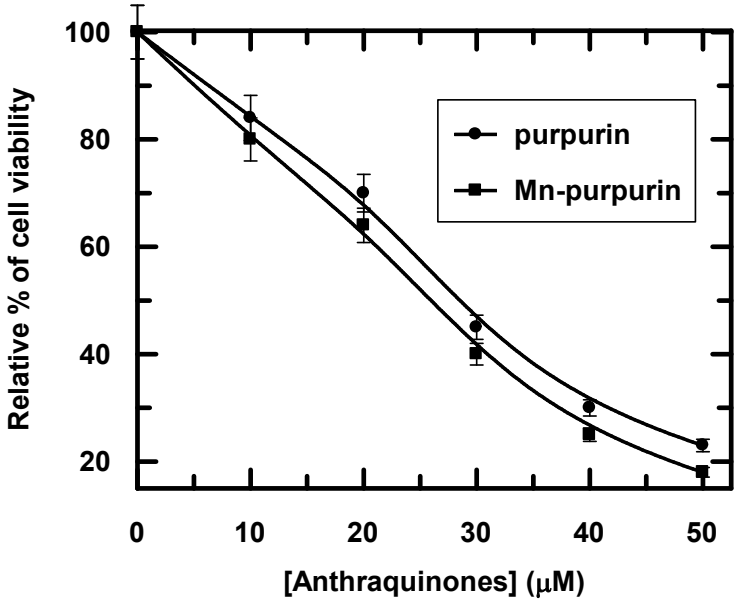

Fig. S9: Dose response curve for the effects of LH_3 and $Mn^{II}(LH_2)_2$ on MOLT-4 cells. In both cases, MOLT-4 cells were treated with the compounds for 72 hours and MTT assay was performed.

References:

1) P. S. Guin, S. Das, P. C. Mandal, J. Inorg. Biochem. 103 (2009) 1702.
2) S. Mukherjee, P. Das, S. Das, J. Phy.Org. Chem. 25 (2012) 385.
3) S. Roy, R. Banerjee, M. Sarkar, J. Inorg. Biochem. 100 (2006) 1320.
4) S. Chakraborti, B. Bhattacharyya, D. Dasgupta, J. Phys. Chem. B 106 (2002) 6947.
5) G. Scatchard, Ann. N. Y. Acad. Sci. 51 (1949) 660.
6) P. Das, P. S. Guin, P. C. Mandal, M. Paul, S. Paul**,** S. Das, J. Phy.Org. Chem. 24 (2011) 774.
7) S. Das, A. Saha, P. C. Mandal, Talanta 43 (1996) 95.
8) H. Beraldo, A. G. Suillerot, L. Tosi, Inorg. Chem. 22 (1983) 4117.
9) R.G. Parr, W. Yang, *Density Functional Theory of Atoms and Molecules*, Oxford University Press, Oxford, 1989.
10) N. M. O'Boyle, A. L. Tenderholt, K. M. Langner, J. Comp. Chem., 2008, **29**, 839.